Science Advances
AAAS

advances.sciencemag.org/cgi/content/full/5/4/eaaw0120/DC1

Supplementary Materials for

Enhancing superconductivity in $SrTiO_3$ films with strain

Kaveh Ahadi*, Luca Galletti, Yuntian Li, Salva Salmani-Rezaie, Wangzhou Wu, Susanne Stemmer

*Corresponding author. Email: kahadi@mrl.ucsb.edu

Published 26 April 2019, *Sci. Adv.* **5**, eaaw0120 (2019)
DOI: 10.1126/sciadv.aaw0120

This PDF file includes:

Supplementary Materials

X-ray diffraction (XRD) and reciprocal space mapping

High-resolution XRD using a Philips Panalytical X'Pert thin-film diffractometer with Cu K^{α} radiation was used for ex-situ characterization of the films. A representative 2θ-ω scan of a $SrTiO_3$ film around the 001 reflection is shown in fig. S1. Laue (thickness) fringes can be seen, indicating smooth films with high crystalline quality. The out-of-plane lattice parameter is 3.93±0.001 Å, as expected for a fully strained $SrTiO_3$ film on LSAT.

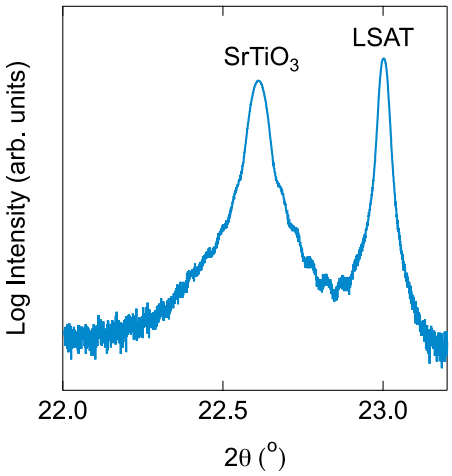

Fig. S1. 2θ-ω scan of a $SrTiO_3$ film on LSAT near the 001 reflections. Figure S2 shows a representative reciprocal space map (RSM) of a $SrTiO_3$/LSAT heterostructure around the 113 film reflection. The axes denote the out-of-plane ($\mathbf{q}_z$) and in-plane ($\mathbf{q}_x$) reciprocal lattice vectors, scaled as $2\pi/a$, where a is the real-space lattice spacing of the respective planes. The RSM shows that the in-plane lattice parameter of the $SrTiO_3$ film is coherently strained to that of the LSAT substrate (a = 3.868 Å).

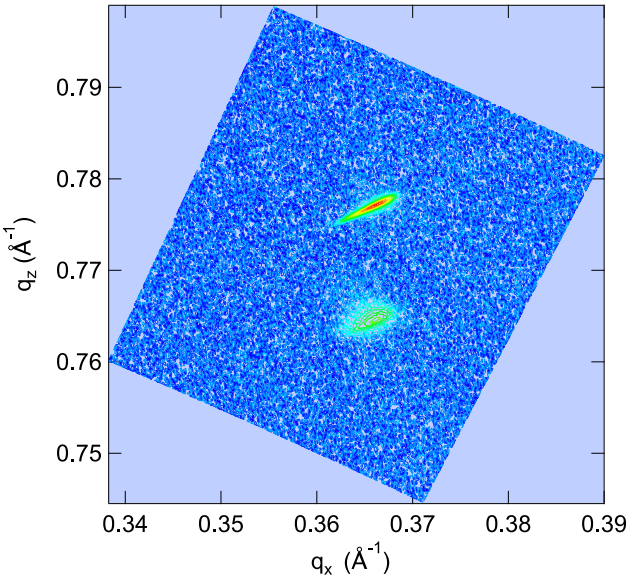

Fig. S2. RSM of a $SrTiO_3$/LSAT heterostructure around the 113 reflection.

Transmission electron microscopy

Figure S3 shows a cross-section high-angle annular dark-field (HAADF) imaging in scanning transmission electron microscopy (STEM) image of a $SrTiO_3$/LSAT heterostructure. The sample was prepared using a FEI Helios Dualbeam Nanolab 650 focused ion beam (FIB) system with a final milling energy of 5 keV Ga ions. A FEI Titan S/TEM at 300 kV with the convergence angle of 9.6 mrad was used for the imaging. The interface between the LSAT substrate and Sm:$SrTiO_3$ is atomically abrupt. Low magnification images (not shown) showed no extended defects, as expected for a coherently strained film.

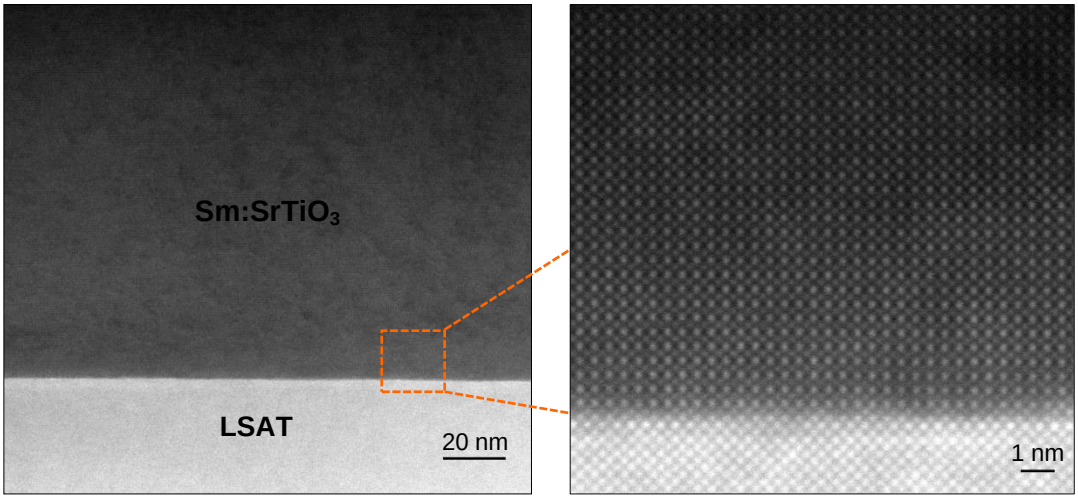

Fig. S3. Cross-sectional HAADF-STEM images.

Measurements of the critical field

Figure S4 shows R_{xx} as a function of an out-of-plane applied magnetic field for three of the films discussed in the main text. Upper magnetic critical fields (H_{C2}) are defined as the intersection with the field axis of the linear extrapolation of the slope in the transition and superconducting states.

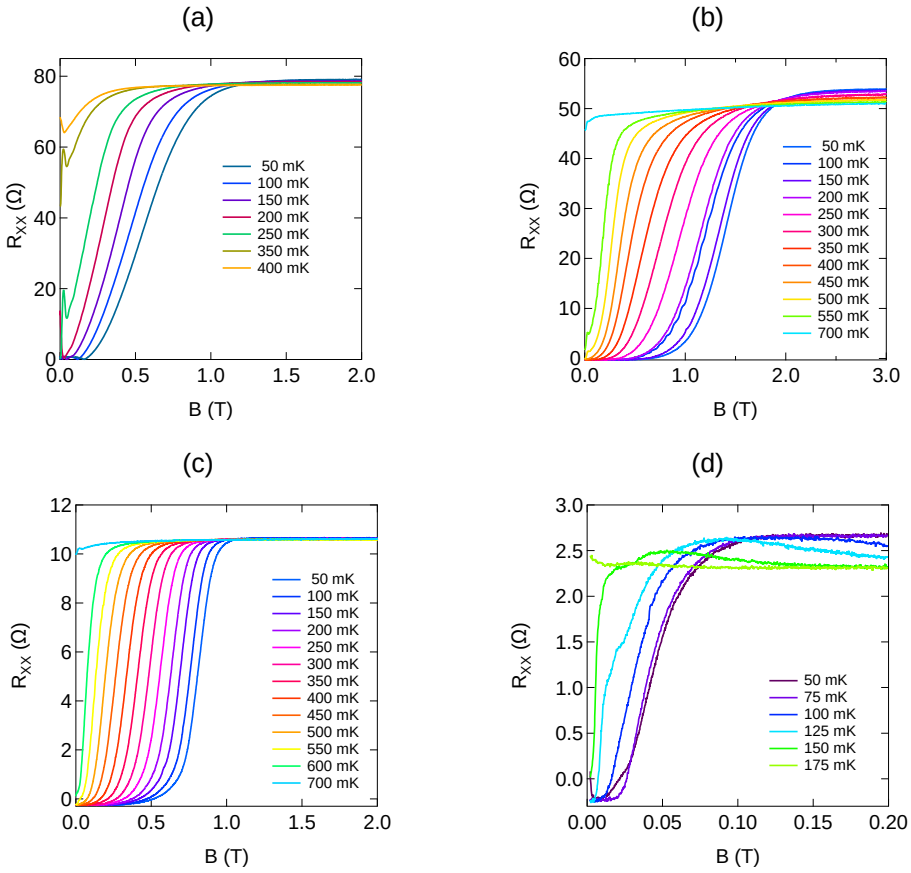

Fig. S4. Magnetic field dependence of the superconducting transition for films with carrier densities of (a) 2×10^{19} cm^{-3}, (b) 6×10^{19} cm^{-3}, (c) 1.4×10^{20} cm^{-3} and (d) 2.8×10^{20} cm^{-3}.

Superconducting transitions and normal state transport for Sm- and La-doped $SrTiO_3$ films grown on $SrTiO_3$ substrates

Figure S5 shows measurements of R_{xx} at temperatures between 400 mK and 10 mK for Sm- and La-doped films grown by MBE on $SrTiO_3$ single crystals. The carrier densities for these films at 2 K were 7.1×10^{19} cm^{-3} and 8.4×10^{19} cm^{-3}, respectively. Their transition temperatures are shown in Fig. 3 in the main text.

Figure S6 shows the additional data for the temperature dependence of the resistivities of additional Sm-doped $SrTiO_3$ films on $SrTiO_3$ substrates. The residual resistivity ratios (RRR) are comparable to those of La-doped $SrTiO_3$ films (cf. ref. 37 in the main text).

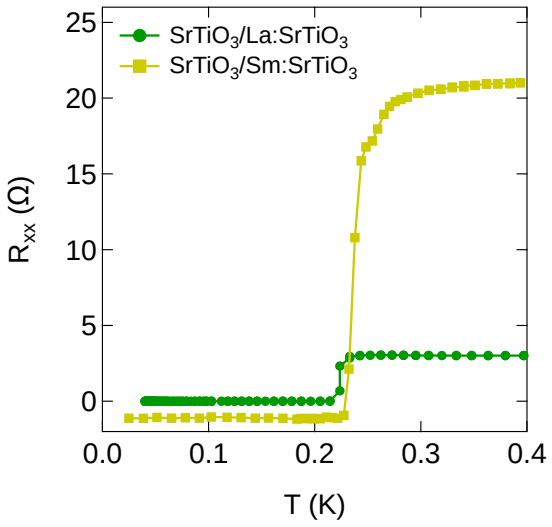

.

Fig. S5. Superconducting transitions for Sm- and La-doped $SrTiO_3$ films grown on $SrTiO_3$ substrates.

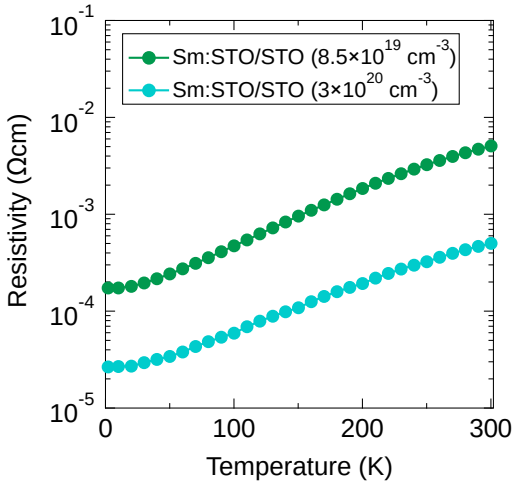

Fig. S6. Resistivity as a function of temperature for Sm-doped $SrTiO_3$ films grown on $SrTiO_3$ substrates.